Raman Spectroscopy of Random Dimerized Domains in 1D Spin Chains

Sami Hakani

January 4, 2022

1 Introduction

A complete understanding of a physical phenomenon must include an understanding of its dynamics: how it changes in time. One burgeoning area of condensed matter physics where dynamics are actively studied is in the magnetic excitations of frustrated spin systems [1]. Such spin systems can host exotic quantum liquid phenomena including fractional excitations, emergent gauge fields, and novel particle statistics. In addition to broadening basic scientific knowledge, understanding the dynamics of frustrated magnetic systems can further technological applications in quantum computing [2].

In 1D systems, where quantum fluctuations are greatly enhanced, dynamics of magnetic excitations can be more readily studied. One technique that has shown great utility in this endeavor is inelastic Raman spectroscopy [3]. While significant research has been performed in studying magnetic phenomena of 1D spin chains using inelastic Raman spectroscopy [4–16], the collection of spin systems probed has been limited to simple 1D spin chains and Spin-Peierls dimerized chains. To better understand magnetic phenomena of 1D magnetic systems, there is a need to study more complex spin chains. While synthesis of unique materials presents one route to this end, inelastic Raman scattering itself could also satisfy this need.

One underappreciated feature of Raman spectroscopy is the interplay between spatial geometry and spin degrees of freedom. In particular, the relative orientation of incident and scattered photon polarizations with respect to a sample's crystallographic axes allows the inelastic Raman scattering spectrum to probe the ground state dynamics of operators besides the Hamiltonian. Even for simple geometries, such as a zig-zagged spin chain, these operators can possess different symmetries from the Hamiltonian. This begs the question as to whether one can use a given spin system with a fixed Hamiltonian to study qualitatively different spin phenomena by simply engineering the dynamical operator.

In this proposal, I will present a theoretical approach to study the interplay between spatial geometry and inelastic Raman spectroscopy. I will first review some basic facts about magnetic insulators. Then, I will introduce the notion of a *quantum liquid* (QL) in 1D, 2D, and 3D materials as a particular phase of magnetic insulators. I will also briefly review some rich tools available to physicists to experimentally probe the exotic magnetic excitations of these phases. I will focus on inelastic Raman spectroscopy and discuss how it has been used to study magnetic excitations in 1D spin chains. Then, I will present my research aims in deducing the Raman response of spatial defects in zig-zagged 1D spin chains. Finally, I will finally present my work thus far [17] which uses a mean-field approach [18] to predicting inelastic Raman scattering spectra of 1D systems.

2 Literature Review

2.1 Magnetic Insulators

Qualitatively, a *magnetic insulator* is a material which does not conduct electric current but does demonstrate magnetic phenomena. We can characterize a magnetic insulator in the limit of a metal described by simplified fermionic Hubbard Hamiltonian

$$H_{\text{Hubbard}} = -t \sum_{\langle i,j\rangle,\sigma} \left(c^\dagger_{i\sigma} c_{j\sigma} + h.c. \right) + U \sum_i n_{i\uparrow} n_{i\downarrow} \tag{1}$$

where $t, U > 0$ have units of energy, $\langle i, j\rangle$ enumerate nearest neighbor lattice sites, $\sigma \in \{\uparrow, \downarrow\}$, $\{c_{i\sigma}, c^\dagger_{j\sigma'}\} = \delta_{ij}\delta_{\sigma\sigma'}$, and $n_{i\sigma} = c^\dagger_{i\sigma} c_{i\sigma}$ is a density operator. With this identification, a magnetic insulator is governed by H_{Hubbard} in the limit $t/U \ll 1$. In this limit, the Hubbard model approximately reduces[1] to the Heisenberg model

$$H_{\text{Heisenberg}} = J \sum_{\langle i,j\rangle} \mathbf{S}_i \cdot \mathbf{S}_j \tag{2}$$

where J is an energy scale. For $J < 0$, we say the system is *ferromagnetic*, while for $J > 0$ we say the system is *antiferromagnetic*. Within the $(t/U) \ll 1$ limit, the Hamiltonian for a given system has SU(2) symmetry.

The Heisenberg model demonstrates a magnetic phase transition on square lattices. At temperatures where $k_B T \ll |J|$, rotational symmetry is spontaneously broken, and the system magnetically orders. Simple examples of order parameters for this phase transition include the magnetization $\mathbf{M} = \sum_j \mathbf{S}_j$ for ferromagnetic materials, or the staggered magnetization $\mathbf{M}_s = \sum_j (-1)^j \mathbf{S}_j$ for antiferromagnetic materials. In the $T \to \infty$ limit, the system is in the normal state ($\mathbf{M}, \mathbf{M}_s = \mathbf{0}$), while in the $T \to 0$ limit the (anti)ferromagnetic system is in the ordered state with a net nonzero (staggered) magnetization. Ferromagnetic order has parallel nearest neighbor spins, while antiferromagnetic or *Néel order* has anti-parallel nearest neighbor spins. While classical magnetic insulators can be understood within this simple framework, quantum mechanical effects and richer lattice geometries in real magnetic insulators can bear highly nontrivial phenomena.

2.2 Quantum Liquid Phenomenology and Contraindicators

A collection of quantum mechanically induced effects within magnetic insulators are theorized to produce exotic phases of matter known as a *quantum liquids* (QLs): (sliding) Luttinger liquids [19], quantum spin liquids [1], Bose-Luttinger liquids [20], etc. While at the time of writing this proposal there is no agreed upon definition of a QL, there are, however, ways to classify what it is not.

Unlike classical magnetic insulators, QLs do not magnetically order. One way a magnetic insulator may fail to order is if it has antiferromagnetic interactions and *geometric frustration*. The canonical example of a geometrically frustrated system is given by the case of an antiferromagnet on a 2D triangular lattice [1]. Because the three corners of a given triangle are all pairwise nearest neighbors, any ground state of the system will have one of the three spins on every triangle parallel to one of its neighbors. Due to this geometric frustration, the classical ground state degeneracy of the 2D triangular antiferromagnet is extensive in the system size.

[1] One can show this using second order perturbation theory on H_{Hubbard} at half filling. In this limit, $H_{\text{Heisenberg}}$ is an effective Hamiltonian with the same spectrum as H_{Hubbard} restricted to its ground state manifold.

Geometrically frustrated quantum antiferromagnets analogously exhibit extensive ground state degeneracies. A seminal example of this property is in the resonating valence bond state proposed by Anderson [21]. One ground state for the aforementioned 2D triangular antiferromagnet is a product state of nearest neighbor singlets known as the valence bond solid. This state, however, does not account for all the symmetries of the Hamiltonian. By accounting for the full symmetries of the Heisenberg Hamiltonian, Anderson constructed the resonating valence bond (RVB) state. The RVB ground state has been shown to be the ground state of many Hamiltonians, and it is a canonical example of a quantum spin liquid.

In addition to quantum spin liquids, other exotic QL phases have been identified that offer explanations for why some magnetic insulators fail to order at low temperatures. One such example is the Luttinger liquid which occurs in 1D systems. Similar to the quantum spin liquid, the Luttinger liquid does not demonstrate spontaneous symmetry breaking of its parent Hamiltonian. Indeed, quantum fluctuations in 1D are so pronounced that they destroy any magnetic ordering. As of late, coupled Luttinger liquids have also generated interest as they can lead to sliding Luttinger liquid phase beyond the Fermi liquid paradigm.

2.3 Theoretical Probes of Magnetic Excitations

Several theoretical tools are also available to predict the scattering spectra for quantum liquid candidates. Here, I briefly touch upon those used in predicting inelastic Raman scattering spectra. One analytic technique, bosonization [22], uses field theoretic tools to compute low energy dynamics for a given system. Another analytic technique includes mean-field approximations [18, 23]. In contrast, mean-field tools can be used to compute higher energy dynamics, and they are often more tractable in execution. Computational techniques such as exact diagonalization [24] and density matrix renormalization group (DMRG) [25] can further supplement analytic techniques.

2.4 Inelastic Raman Spectroscopy

The rich magnetic phenomenology of quantum liquids can be probed through inelastic Raman scattering. In this section, I review fundamentals of this technique. In a magnetic Raman scattering process, an incident photon with frequency ω_i indirectly creates magnetic excitations [3]. The photon first excites a virtual particle-hole pair. This virtual pair then annihilates into magnetic excitations and a scattered photon with frequency ω_f. The inelastic Raman scattering spectrum $I(\omega)$ is measured with respect to the Raman shift $\omega = \omega_f - \omega_i$. While the Raman scattering process involves virtual charge excitations, it can be solely described in terms of a spin Hamiltonian within London-Fleury theory [26]. In brief, typical Raman scattering experiments are carried out at Raman shifts well below the charge gap [3] which effectively freezes out the electronic degrees of freedom.

Within London-Fleury theory, the scattering spectrum $I(\omega)$ is the frequency space representation of the time correlation function of an operator R [22].

$$I(\omega) = \frac{1}{2\pi} \int_{-\infty}^{\infty} dt \; e^{i\omega t} \langle R(t) R(0) \rangle \tag{3}$$

Where R is the Loudon-Fleury photon-induced superexchange operator [26]

$$R = \sum_{\mathbf{r}_1, \mathbf{r}_2} (\hat{\mathbf{e}}_i \cdot \mathbf{r}_{12})(\hat{\mathbf{e}}_s \cdot \mathbf{r}_{12}) A(\mathbf{r}_{12}) \mathbf{S}_{r_1} \cdot \mathbf{S}_{r_2} \tag{4}$$

Above, $\hat{\mathbf{e}}_{i,s}$ is the polarization direction of the scattered photon and $\mathbf{r}_{12} = \mathbf{r}_1 - \mathbf{r}_2$. Generally, $A(\mathbf{r}_{12})$ is difficult to determine, but "the ratio between the factors on different bonds is known to be of

Compound	Reference
$KCuF_3$	[4–7]
$LiCu_2O_2$	[8]
Sr_2CuO_3	[9]
$SrCuO_2$	[9]
$CuGeO_3$	[10–16]

Table 1: Compounds whose magnetic excitations have been probed using Raman spectroscopy.

the same order as that between the exchange couplings on those bonds" [22]. For brevity, we refer to R as the Raman operator.

For inelastic scattering, it is clear[2] from (3) and (4) that two different Raman operators R, R' yield the same spectrum if $R' = R - CH_0$ for some constant C. That is, the only part of the Raman operator which contributes to the inelastic scattering spectrum is the part which does not commute with H_0. Therefore, we will say two Raman operators R, R' are *spectrally equivalent* whenever $R' = R - CH_0$ for arbitrary $C \in \mathbb{R}$.

2.5 Raman Studies on 1D Materials

In this section, I review Raman spectroscopy studies done on 1D magnetic insulators. Table 1 contains an incomplete list of several compounds whose magnetic excitations have been probed using Raman spectroscopy.

Raman spectroscopy of $KCuF_3$ has demonstrated the utility of inelastic Raman scattering in probing magnetic excitations. In particular, below the Néel temperature of $KCuF_3$, Raman scattering experiments have measured a gapless spinon excitation continuum [5] – a feature characteristic of 1D systems. Measurements of Sr and Li based materials 1D spin chains [8, 9] have similarly shown spectroscopic features beyond phononic contributions that likely arise from magnetic excitations. In addition to measuring simple 1D chains, Raman spectroscopy has been used to probe magnetic excitations in more exotic 1D systems that magnetically dimerize.

A prototypical Spin-Peierls material is the quasi-1D inorganic compound $CuGeO_3$, which dimerizes at $T_{sp} = 14$ K [18]. Magnetic Raman scattering has been performed on $CuGeO_3$ both above and below T_{sp} [10–15]. In the uniform phase $T_{sp} < T$, a broad continuum attributed to four-spinon excitations has been observed. In the dimerized phase, spectroscopic features previously attributed to magnetic excitations have been determined to be due to phononic excitations [16].

[2] If $[R, H_0] = 0$, then $[R, U(t)] = 0$, where $U(t) = e^{iH_0 t}$. Since $R(t) = U(t)R(0)U^\dagger(t)$, we have $\langle R(t)R(0)\rangle = \langle R(0)^2\rangle$. We can pull this term out of the integral so that $I(\omega) = \langle R(0)^2\rangle\, \delta(\omega)$ which is a trivial spectrum.

3 Proposed Work

3.1 Research Aims

In order to deduce the Raman response of spatial defects in zig-zagged 1D spin chains, I aim to first characterize the family of Raman operators produced in this geometry. As a practical example, I will approach this problem by studying the Raman response of a recently discovered quasi-2D spin-1/2 material $Ba_4Ir_3O_{10}$ [27] by treating the material as consisting of decoupled 1D spin chains [17]. While the material itself is not 1D, it has been argued to be fruitfully modeled in terms of coupled 1D Heisenberg chains [27], and this limit provides a tractable model for studying dynamics of fractional spinon excitations.

In addition to tabulating the Raman operators in this geometry, another step towards characterizing dynamics of dimerized domains includes determining the Raman response of these Raman operators. As a first step, I will use a standard mean-field approximation of free 1D spinons [18] in order to compute the four spinon contribution to the inelastic scattering spectrum. Raman spectroscopy measurements of this material [17] provide an excellent comparison for the mean-field results.

In addition to studying the Raman response of $Ba_4Ir_3O_{10}$, I will also compute the Raman response of the remaining Raman operators arising from 1D zig-zagged chains. I have already found that zig-zagged spin chains can give rise to Raman operators reminiscent of Spin-Peierls dimerized Hamiltonians. By introducing spatial defects into the zig-zagged spin chains, one could construct a Raman operator with dimerized domains. As of yet, no Raman spectroscopy studies have been performed on 1D spin chains with random dimerized domains. Such systems are known give rise to random singlet phases [28], where isolated spins at the domain walls of dimerized domains can engage in long range entanglement by forming singlet states. The Raman response of these isolated spins, however, is not well understood. Such a system could potentially be studied by proxy through Raman spectroscopy of 1D zig-zag chains with spatial defects, thereby shedding light on long range entanglement in condensed matter systems.

For example, analytic mean-field approaches will be supplemented with numeric tools specially designed to study 1D spin systems [25, 29]. In tandem, the former will provide insight into the high energy dynamics, while the latter will give insight into systems that are analytically intractable. Numerically studying the Raman response of isolated spins between dimerized domains is one area where computational approaches will be indispensible.

Understanding the interplay between spatial defects and their effect on the Raman response of a spin system could also give insight into previously conducted Raman spectroscopy experiments. In particular, a cohesive theory of this interplay could serve as a discriminator between novel magnetic phenomena and geometric artifacts in a given spectrum.

3.2 Current Progress

3.2.1 Polarization Selection Rules for 1D Zig-Zagged Chains

In studying the quantum liquid candidate $Ba_4Ir_3O_{10}$ [17], I have tabulated polarization selection rules for inelastic Raman spectroscopy of 1D zig-zagged spin chains. As a minimal model for this material, consider the antiferromagnetic J_1-J_2 Hamiltonian in 1D

$$H_0 = \sum_j J_1 \mathbf{S}_j \cdot \mathbf{S}_{j+1} + J_2 \mathbf{S}_j \cdot \mathbf{S}_{j+2} \tag{5}$$

for $J_1 \geq J_2 \geq 0$. We will further allow the 1D chain to be zig-zagged and parametrized by an angle

θ_0 as in Fig. 1. Note, a zig-zag chain does not affect H_0, but it will affect the form of the Raman

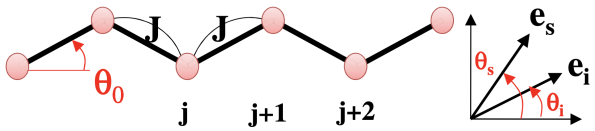

Figure 1: Bond and polarization angle parametrization [22].

operator.

We choose to work in this minimal model since the elementary excitations for (5) are spinons. Moreover, in the $J_2 \to 0$ and $\theta_0 \to 0$ limits independently, we also obtain Hamiltonians whose elementary excitations are fractional. Using the coordinates provided in Fig. 1, we proceed to compute the Raman operators for various input and output photon polarizations. We find[3]

$$R = A_1 \left[f(\theta_i, \theta_s, \theta_0) \sum_j \mathbf{S}_j \cdot \mathbf{S}_{j+1} + h(\theta_i, \theta_s, \theta_0) \sum_j (-1)^j \mathbf{S}_j \cdot \mathbf{S}_{j+1} \right] + A_2 g(\theta_i, \theta_s, \theta_0) \sum_j \mathbf{S}_j \cdot \mathbf{S}_{j+2} \tag{6}$$

For

$$f(\theta_i, \theta_s, \theta_0) = \cos\theta_i \cos\theta_s \cos^2\theta_0 + \sin\theta_i \sin\theta_s \sin^2\theta_0 \tag{7}$$

$$h(\theta_i, \theta_s, \theta_0) = \frac{1}{2} \sin(2\theta_0) \sin(\theta_i + \theta_s) \tag{8}$$

$$g(\theta_i, \theta_s, \theta_0) = 4 \cos\theta_i \cos\theta_s \cos^2\theta_0 \tag{9}$$

and $A_2/A_1 \sim \mathcal{O}(J_2/J_1)$. We next consider limiting cases of (5) and compute the associated Raman operator for different bare Hamiltonians. In doing so, we will find selection rules based on photon polarization angles.

For concreteness, consider the orientation of a $Ba_4Ir_3O_{10}$ crystal as in Fig. 2. The effective 1D chain is highlighted in purple and lies in bc-plane. Let θ_0 be the angle made by bonds with respect to the c-axis and $\theta_{i,s}$ parametrize the photon polarization direction as in Fig. 1. Thus, a bb polarization amounts to $\theta_i = \theta_s = -\pi/2$, while a bc polarization amounts to $\theta_i = -\pi/2$ and $\theta_s = 0$.

Using the results of the previous sections, we summarize the polarization selection rules for Raman scattering of different bare Hamiltonians in Table 2.

3.2.2 Spinon Mean-Field Calculation of Raman Spectra for $Ba_4Ir_3O_{10}$

Within mean field, the inelastic scattering spectrum can be computed[4] following Brenig [18]. Up to spectral equivalence, the Raman operator for the J_1-J_2 model can be transformed using Jordan-Wigner fermionization. We write (for unit lattice spacing)

$$S_j^+ = c_j^\dagger \exp\left[-i\pi \sum_{i=1}^{j-1} c_i^\dagger c_i \right], \quad S_j^- = \exp\left[i\pi \sum_{i=1}^{j-1} c_i^\dagger c_i \right] c_j, \quad S_j^z = c_j^\dagger c_j - \frac{1}{2} \tag{10}$$

[3] See Appendix A.
[4] See Appendix B.

Polarization In	Polarization Out	Zig-Zag	J_2	H	R	Equivalent R
not c	any	none	none	H_1	0	0
any	not c	none	none	H_1	0	0
c	c	none	none	H_1	H_1	0
a	any	yes	none	H_1	0	0
any	a	yes	none	H_1	0	0
b	b	yes	none	H_1	0	0
b	c	yes	none	H_1	$H_1 + R_D$	R_D
c	b	yes	none	H_1	$H_1 + R_D$	R_D
c	c	yes	none	H_1	0	0
not c	any	none	yes	H_0	0	0
any	not c	none	yes	H_0	0	0
c	c	none	yes	H_0	H_0	H_0
a	any	yes	yes	H_0	0	0
any	a	yes	yes	H_0	0	0
b	b	yes	yes	H_0	H_1	H_0
b	c	yes	yes	H_0	R_D	R_D
c	b	yes	yes	H_0	R_D	R_D
c	c	yes	yes	H_0	H_0	H_0

Table 2: Polarization selection rules for Raman scattering of various bare Hamiltonians. The H column gives the Hamiltonian ($H_1 = J\sum_j \mathbf{S}_j \cdot \mathbf{S}_{j+1}$ having only 1st neighbor interactions while $H_0 = H_1 + J\alpha\sum_j \mathbf{S}_j \cdot \mathbf{S}_{j+2}$ having both 1st and 2nd neighbor interactions). The R column gives the general form of the full Raman operator (H_1, H_0, or a dimerization term $R_D \propto \sum_j (-1)^j \mathbf{S}_j \cdot \mathbf{S}_{j+1}$). A sum in this column refers to a linear combination of two different operators. The rightmost column gives the Raman operator up to spectral equivalence for the corresponding Hamiltonian. Equivalent Raman operators in the H_0 class are the only cases where the inelastic Raman scattering spectrum can be used to observe spinon excitations.

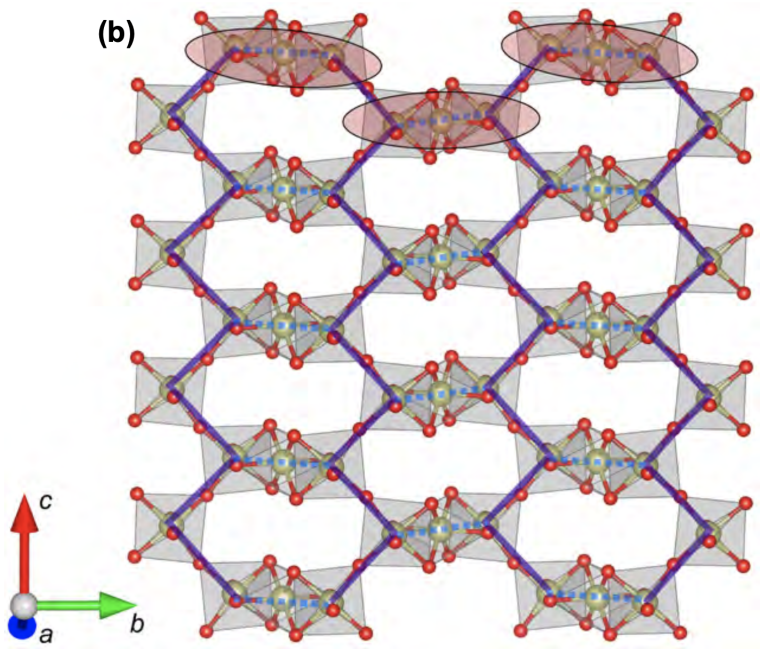

Figure 2: Sample $Ba_4Ir_3O_{10}$ crystal coordinate system [27]. 1D chains are highlighted in purple.

with $\{c_j, c_{j'}^\dagger\} = \delta_{jj'}$ and all other anticommutators zero. For R_ν ($\nu = 1, 2$), one finds[5]

$$R_\nu \propto \sum_{k,k',q} h^{(\nu)}(k, k', q) c_k^\dagger c_{k+q} c_{k'}^\dagger c_{k'-q} + \Lambda_{1\text{ph}}^{(\nu)} \tag{11}$$

where[6]

$$h^{(2)}(k, k', q) = \cos(2q) - \cos(2k + q) - \cos(2k' - q), \quad \Lambda_{1\text{ph}}^{(2)} = \sum_j \frac{1}{2}(c_j^\dagger c_{j+2} + h.c.) + \frac{1}{4} - c_j^\dagger c_j \tag{12}$$

and

$$h^{(1)}(k, k', q) = \cos(q), \quad \Lambda_{1\text{ph}}^{(1)} = \sum_j \frac{1}{2}(c_j^\dagger c_{j+1} + h.c.) + \frac{1}{4} - c_j^\dagger c_j \tag{13}$$

Within mean-field, $\Lambda_{1\text{ph}}^{(\nu)}$ does not contribute to the inelastic scattering spectrum [18]. Having expressed the Raman operators in terms of fermionic operators, we may now proceed to compute the autocorrelation function of R_ν in imaginary time $\tau = it$. We use the dispersion relation for spinons

$$\epsilon_k = t \cos k, \quad t = -\frac{\pi}{2} J_{\text{eff}} \tag{14}$$

and the Fermi function

$$f(\epsilon_k) = \frac{1}{\exp(\beta \epsilon_k) + 1} \tag{15}$$

[5] See Appendix B.

[6] Note: here, the $\Lambda_{1\text{ph}}$ term is written in real space.

with $\beta = 1/T$ as inverse temperature[7]. One finds[8]

$$\langle R_\nu(\tau)R_\nu(0)\rangle \propto \left[\sum_{k,k',q} h^{(\nu)}(k,k',q)f(\epsilon_k)(1-f(\epsilon_{k+q}))f(\epsilon_{k'})(1-f(\epsilon_{k'-q}))e^{-\tau(\epsilon_{k+q}+\epsilon_{k'-q}-\epsilon_k-\epsilon_{k'})}\right] \times 2\left[h^{(\nu)}(k,k',q) - h^{(\nu)}(k,k',k'-k-q)\right] \tag{16}$$

Having found the Wick decomposition, we now use the autocorrelation function (16) to compute the inelastic Raman scattering spectrum. We integrate over t first with the phase $e^{i(\omega-\Delta\epsilon)t}$, where $\Delta\epsilon = \epsilon_{k+q} + \epsilon_{k'-q} - (\epsilon_k + \epsilon_{k'})$ is the change in spinon energy after a 2 body scattering process. This gives a factor of

$$\sum_{k'} \delta(\omega - \Delta\epsilon) \approx \frac{1}{2\pi}\int dk'\ \delta(\omega-\Delta\epsilon) = \frac{1}{2\pi}\sum_{k'} \frac{1}{\sqrt{(2t\sin(q/2))^2 + (\epsilon_{k+q}-\epsilon_k-\omega)^2}} \tag{17}$$

where the second sum on the RHS is over $k' \in [-\pi, \pi]$ that satisfy

$$\sin(k'-q/2) = \frac{\epsilon_{k+q}-\epsilon_k-\omega}{2t\sin(q/2)} \tag{18}$$

Taking the continuum limit on k, q as well, one finds the spectrum for R_ν

$$I^{(\nu)}(\omega) \propto \int_{-\pi}^{\pi} dk \int_{-\pi}^{\pi} dq \sum_{k'} \frac{h^{(\nu)}(k,k',q)[h^{(\nu)}(k,k',q) - h^{(\nu)}(k,k',k'-k-q)]}{\sqrt{(2t\sin(q/2))^2 + (\epsilon_{k+q}-\epsilon_k-\omega)^2}} \times f(\epsilon_k)(1-f(\epsilon_{k+q}))f(\epsilon_{k'})(1-f(\epsilon_{k'-q})) \tag{19}$$

3.2.3 Comparison with Experimental Measurements

The spinon mean-field calculation of the inelastic Raman scattering spectrum (19) can be numerically integrated to compare with experimental measurements of the quasi-1D spin chains in $Ba_4Ir_3O_{10}$. In Ref. [17], we compare the imaginary part of the Raman susceptibility $\chi''_{R_\nu,R_\nu}(\omega)$ with experimental measurements. The susceptibility is related to the intensity via $I(\omega) = \chi''(\omega)/(1-e^{-\omega/T})$ [18].

At low temperatures ($k_BT/J_{\text{eff}} < 1$), the mean-field spectra arising from both R_1 and R_2 qualitatively agree with experimental measurements, as seen in Fig. 3. At high temperatures ($k_BT/J_{\text{eff}} > 1$), the mean-field susceptibilities for R_1 and R_2 become qualitatively different as shown in Fig. 4. This difference quantifies the self-consistency breakdown of the mean-field theory at high temperatures.

3.2.4 Spinon Mean-Field Theory for Dimerized Raman Operators

To better understand the Raman response of dimerized systems, I have also used spinon mean-field theory to compute the inelastic scattering spectrum arising from a dimerized Raman operator for a nearest neighbor Heisenberg Hamiltonian. This Raman response would arise, for example, for a 1D zig-zag chain with nearest neighbor interactions when considering the bc or cb polarization (in Table 2, $H = H_1$ and the equivalent $R = R_D$).

[7] Note: units are chosen such that $\hbar = c = k_B = 1$.

[8] See Appendix B.

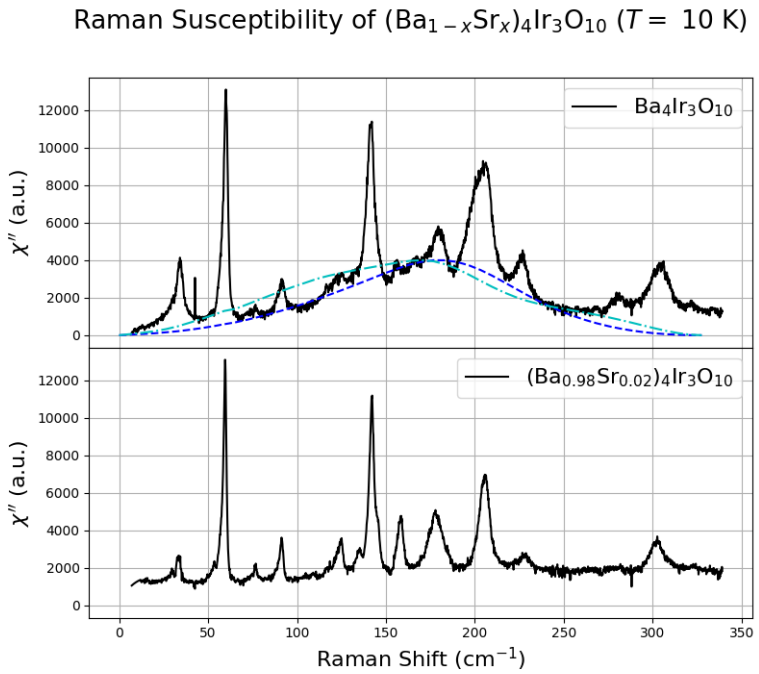

Figure 3: Raman susceptibility of quantum liquid candidate $Ba_4Ir_3O_{10}$ and a sister compound $(Ba_{0.98}Sr_{0.02})_4Ir_3O_{10}$ at $T = 10$ K plotted with spinon mean-field calculated susceptibilities χ''_{R_1,R_1} (blue, dashed) and χ''_{R_2,R_2} (cyan, dot-dashed) ($J_{\text{eff}}/k_B \approx 75$ K) [17]. Non-magnetic Sr substitution produces magnetic order in the sister compound and eliminates the four-spinon continuum.

Within this theory, the quadratic fermionic terms reminiscent of $\Lambda^{(\nu)}_{\text{1ph}}$ *do* contribute to the scattering spectrum within mean-field. In particular, one finds the quadratic fermionic terms to be

$$\Lambda = \sum_k i \sin(k) c^\dagger_{k+\pi} c_k \tag{20}$$

Following the same approach as for R_ν, I exactly find[9] the Raman susceptibility arising from $R = \Lambda$ to be

$$\chi''_{\Lambda,\Lambda}(\omega) = \frac{1}{4\pi t}\sqrt{1-\left(\frac{\omega}{2t}\right)^2}\tanh(\beta\omega/4) \tag{21}$$

for $\omega > 0$ and $\beta = 1/k_B T$. Within linear response theory, this susceptibility agrees with the first order sum rule $\int_{-\infty}^{\infty} d\omega\ \omega\chi''(\omega) = -\pi \langle[[H_1, \Lambda], \Lambda]\rangle$ at finite temperature.

3.3 Future Work

In preparation to study the Raman response of random dimerized domains, I will begin by numerically computing the inelastic scattering spectrum for small finite chains using the density matrix renormalization group (DMRG) algorithm [25]. Calculations will be performed using the TeNPy Library [29] and carried out on various computing resources ranging from local machines to GaTech supercomputing clusters.

[9] See Appendix C.

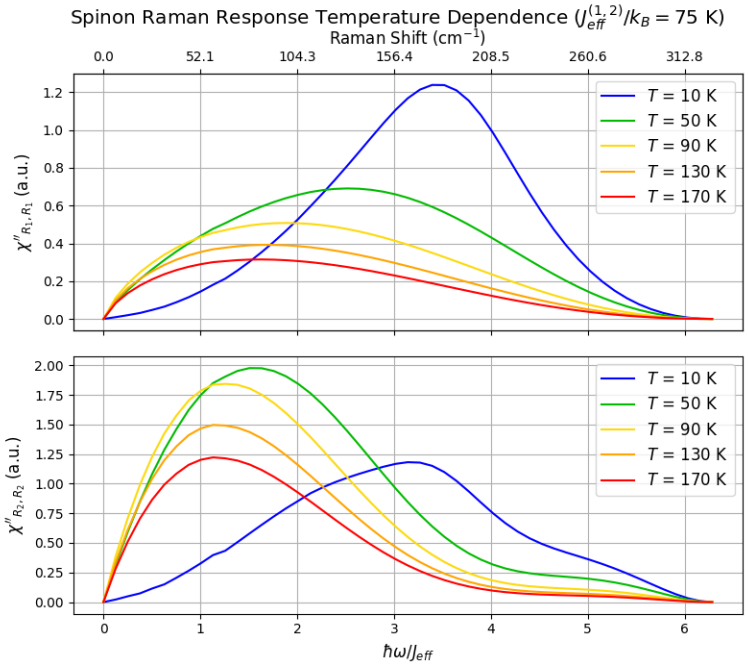

Figure 4: Spinon Raman response computed within two mean field choices $R_{\nu=1,2}$, with $J_{\text{eff}}^{\nu=1,2}/k_B = 75$ K at various temperatures [17].

4 Conclusion

Thus far, I have performed preliminary work towards understanding the interplay between spatial geometry and inelastic Raman spectroscopy. In exploring the Raman response of $Ba_4Ir_3O_{10}$, I found that zig-zagged 1D spin chains can possess London-Fleury Raman operators reminiscent of Spin-Peierls dimerized Hamiltonians. Using a mean-field theory of free spinons, the inelastic scattering spectrum can be deduced as a measure of the dynamics of a given Raman operator. That a non-dimerized material can be used to study dynamics of a dimerized operator begs the question of whether more exotic dynamics not exhibited by the Hamiltonian of a system can be studied by introducing spatial defects into a crystal.

Through analytic and computational techniques, I propose to study the dynamics of random dimerized domains in 1D spin chains by proxy using this unique role of spatial geometry in determining the inelastic Raman scattering spectrum. As a proof of principle, this study will determine the practicality of engineering Raman operators to study dynamics of spin systems that have yet to be probed or synthesized. Moreover, it has the potential to shed light on the role of long range entanglement of isolated spins that exist in the domain walls between random dimerized domains.

Studying the dynamics of magnetic excitations in frustrated 1D spin systems is an essential component of understanding quantum liquid phenomena. At this time, there does not exist a complete understanding of the exotic collective behavior of quantum liquids. That such phases of matter are host to interesting and technologically useful features is one of the many reasons to contribute to their study.

References

[1] Leon Balents. Spin liquids in frustrated magnets. *Nature*, 464(7286):199–208, March 2010.

[2] A.Yu. Kitaev. Fault-tolerant quantum computation by anyons. *Annals of Physics*, 303(1):2–30, 2003.

[3] Dirk Wulferding, Youngsu Choi, Wonjun Lee, and Kwang-Yong Choi. Raman spectroscopic diagnostic of quantum spin liquids. *Journal of Physics: Condensed Matter*, 32(4):043001, October 2019. Publisher: IOP Publishing.

[4] I. Yamada and H. Onda. Light scattering from magnetic-energy fluctuations in the one-dimensional Heisenberg antiferromagnet $KCuF_3$. *Physical Review B*, 49(2):1048–1053, January 1994. Publisher: American Physical Society.

[5] V. Gnezdilov, J. Deisenhofer, P. Lemmens, D. Wulferding, O. Afanasiev, P. Ghigna, A. Loidl, and A. Yeremenko. Phononic and magnetic excitations in the quasi-one-dimensional Heisenberg antiferromagnet $KCuF_3$. *Low Temperature Physics*, 38(5):419–427, May 2012. Publisher: American Institute of Physics.

[6] James C. T. Lee, Shi Yuan, Siddhartha Lal, Young Il Joe, Yu Gan, Serban Smadici, Ken Finkelstein, Yejun Feng, Andrivo Rusydi, Paul M. Goldbart, S. Lance Cooper, and Peter Abbamonte. Two-stage orbital order and dynamical spin frustration in $KCuF_3$. *Nature Physics*, 8(1):63–66, January 2012. Bandiera_abtest: a Cg_type: Nature Research Journals Number: 1 Primary_atype: Research Publisher: Nature Publishing Group.

[7] D. A. Tennant, T. G. Perring, R. A. Cowley, and S. E. Nagler. Unbound spinons in the S=1/2 antiferromagnetic chain $KCuF_3$. *Physical Review Letters*, 70(25):4003–4006, June 1993. Publisher: American Physical Society.

[8] K.-Y. Choi, S. A. Zvyagin, G. Cao, and P. Lemmens. Coexistence of dimerization and long-range magnetic order in the frustrated spin-chain system LiCu 2 O 2 : Inelastic light scattering study. *Physical Review B*, 69(10):104421, March 2004.

[9] O. V. Misochko, S. Tajima, C. Urano, H. Eisaki, and S. Uchida. Raman-scattering evidence for free spinons in the one-dimensional spin-1/2 chains of Sr_2CuO_3 and $SrCuO_2$. *Physical Review B*, 53(22):R14733–R14736, June 1996. Publisher: American Physical Society.

[10] V. Kiryukhin and B. Keimer. Incommensurate lattice modulation in the spin-Peierls system $CuGeO_3$. *Physical Review B*, 52(2):R704–R706, July 1995. Publisher: American Physical Society.

[11] P. H. M. van Loosdrecht, J. P. Boucher, G. Martinez, G. Dhalenne, and A. Revcolevschi. Inelastic Light Scattering from Magnetic Fluctuations in $CuGeO_3$. *Physical Review Letters*, 76(2):311–314, January 1996.

[12] Masashi Hase, Ichiro Terasaki, and Kunimitsu Uchinokura. Observation of the spin-Peierls transition in linear Cu^{2+} (spin-1/2) chains in an inorganic compound $CuGeO_3$. *Physical Review Letters*, 70(23):3651–3654, June 1993. Publisher: American Physical Society.

[13] Masayuki Udagawa, Hiroaki Aoki, Norio Ogita, Osamu Fujita, Akio Sohma, Atsuyuki Ogihara, and Jun Akimitsu. Raman Scattering of CuGeO3. *Journal of the Physical Society of Japan*, 63(11):4060–4064, November 1994. Publisher: The Physical Society of Japan.

[14] M. Braden, B. Hennion, W. Reichardt, G. Dhalenne, and A. Revcolevschi. Spin-Phonon Coupling in $CuGeO_3$. *Physical Review Letters*, 80(16):3634–3637, April 1998. Publisher: American Physical Society.

[15] Haruhiko Kuroe, Tomoyuki Sekine, Masashi Hase, Yoshitaka Sasago, Kunimitsu Uchinokura, Hironao Kojima, Isao Tanaka, and Yuki Shibuya. Raman-scattering study of $CuGeO_3$ in the spin-peierls phase. *Phys. Rev. B*, 50:16468–16474, Dec 1994.

[16] I Loa, S Gronemeyer, C Thomsen, and R.K Kremer. Isotope effects in $CuGeO_3$ studied by Raman spectroscopy. *Solid State Communications*, 117(5):279–283, 2001.

[17] Aaron Sokolik, Sami Hakani, Susmita Roy, Nicholas Pellatz, Hengdi Zhao, Gang Cao, Itamar Kimchi, and Dmitry Reznik. Spinons and damped phonons in spin-1/2 quantum-liquid $Ba_4Ir_3O_{10}$ observed by Raman scattering. *arXiv:2110.15916 [cond-mat]*, October 2021. arXiv: 2110.15916.

[18] Wolfram Brenig. Raman scattering from frustrated quantum spin chains. *Physical Review B*, 56(5):2551–2555, August 1997.

[19] Ranjan Mukhopadhyay, C. L. Kane, and T. C. Lubensky. Sliding luttinger liquid phases. *Phys. Rev. B*, 64:045120, Jul 2001.

[20] Ethan Lake, T. Senthil, and Ashvin Vishwanath. Bose-luttinger liquids. *Phys. Rev. B*, 104:014517, Jul 2021.

[21] P. W. Anderson. The resonating valence bond state in la¡sub¿2¡/sub¿cuo¡sub¿4¡/sub¿ and superconductivity. *Science*, 235(4793):1196–1198, 1987.

[22] Masahiro Sato, Hosho Katsura, and Naoto Nagaosa. Theory of Raman Scattering in One-Dimensional Quantum Spin-1/2 Antiferromagnets. *Physical Review Letters*, 108(23):237401, June 2012. Publisher: American Physical Society.

[23] G. Gómez-Santos. Role of domain walls in the ground-state properties of the spin-1/2 *XXZ* Hamiltonian in the linear chain. *Physical Review B*, 41(10):6788–6793, April 1990.

[24] Rajiv R. P. Singh, Peter Prelovšek, and B. Sriram Shastry. Magnetic Raman Scattering from 1D Antiferromagnets. *Physical Review Letters*, 77(19):4086–4089, November 1996. Publisher: American Physical Society.

[25] Steven R. White. Density matrix formulation for quantum renormalization groups. *Phys. Rev. Lett.*, 69:2863–2866, Nov 1992.

[26] P. A. Fleury and R. Loudon. Scattering of Light by One- and Two-Magnon Excitations. *Physical Review*, 166(2):514–530, February 1968.

[27] Gang Cao, Hao Zheng, Hengdi Zhao, Yifei Ni, Christopher A. Pocs, Yu Zhang, Feng Ye, Christina Hoffmann, Xiaoping Wang, Minhyea Lee, Michael Hermele, and Itamar Kimchi. Quantum liquid from strange frustration in the trimer magnet $Ba_4Ir_3O_{10}$. *npj Quantum Materials*, 5(1):1–8, May 2020. Number: 1 Publisher: Nature Publishing Group.

[28] Daniel S. Fisher. Random antiferromagnetic quantum spin chains. *Phys. Rev. B*, 50:3799–3821, Aug 1994.

[29] Johannes Hauschild and Frank Pollmann. Efficient numerical simulations with Tensor Networks: Tensor Network Python (TeNPy). *SciPost Phys. Lect. Notes*, page 5, 2018.